IEEE Photonics Journal
An IEEE Photonics Society Publication

Open Access

Non-Line-of-Sight Location With Gauss Filtering Algorithm Based on a Model of Photon Flight

Volume 12, Number 3, June 2020

Yu Ren
Zongliang Xie
Yihan Luo
Shaoxiong Xu
Haotong Ma
Yi Tan

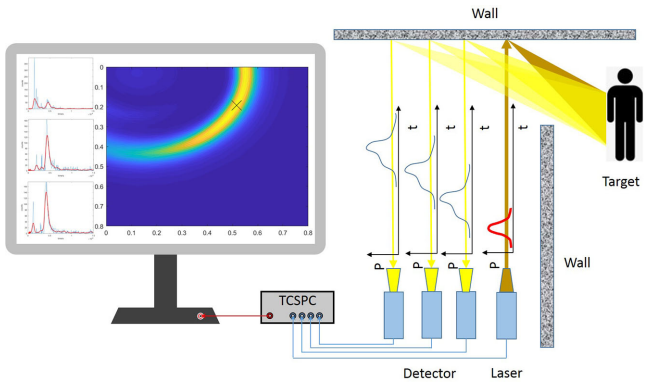

DOI: 10.1109/JPHOT.2020.2994784

Non-Line-of-Sight Location With Gauss Filtering Algorithm Based on a Model of Photon Flight

Yu Ren,[1,2,3] **Zongliang Xie**,[1,2] **Yihan Luo**,[1,2] **Shaoxiong Xu**,[1,2] **Haotong Ma**,[1,2] **and Yi Tan**[1,2]

[1]Institute of Optics and Electronics, Chinese Academy of Science, Chengdu 610209, China
[2]Key Laboratory of Optical Engineering, Chinese Academy of Science, Chengdu 610209, China
[3]University of Chinese Academy of Science, Beijing 100049, China

DOI:10.1109/JPHOT.2020.2994784

Manuscript received March 17, 2020; revised April 23, 2020; accepted May 11, 2020. Date of publication May 14, 2020; date of current version June 22, 2020. This work was supported by the Youth Innovation Promotion Association, CAS (2017428, 2018411, and 2020372), in part by State Key Laboratory of Pulsed Power Laser Technology (SKL2018KF05), in part by Excellent Youth Foundation of Sichuan Scientific Committee (2019JDJQ0012), in part by CAS "Light of West China" Program, and in part by Young Talents of Sichuan Thousand People Program. Corresponding authors: Yihan Luo; Zongliang Xie (e-mail: luo.yihan@foxmail.com; zongliang.xie@yahoo.com).

Abstract: Recently, non-line-of-sight (NLOS) detection based on time of flight (TOF) has been investigated. In order to simulate the NLOS location of a hidden object, we derive the signal scattered by the object and build a model of photon flight based on photon scattering and propagation. To improve the authenticity of the model, the bidirectional reflectance distribution function (BRDF) is used to characterize the scattering process. The Gauss filter is proposed to extract the TOF of the scattering sources of interest without a priori information or manual judgment of the useful scattered signal by filtering the disturbance out of the histogram. The hidden object can then be located by TOF processing. Compared with previous work using a fitting algorithm, the Gauss filtering approach preserves more waveform information and presents improved positioning accuracy and robustness under the influence of noise, which is demonstrated in both simulation and experiment. It is possible to locate a NLOS object automatically through filtering identification of the object signal. The simplicity, high efficiency, and automation of this algorithm make it applicable for tracking a hidden moving object.

Index Terms: Non-line-of-sight detection, Gauss filter, bidirectional reflectance distribution function.

1. Introduction

Non-line-of-sight (NLOS) detection is a method to discover a target that is out of sight. Information about the object, Including its position, velocity, and features, cannot be observed directly, but can be deduced from optical information. This technology has many valuable applications. Its wide application in complex situations such as rescue, autopilot, and anti-terrorist operations could reduce casualties [1]. Furthermore, it could be applied to real-time path planning to assist unmanned devices such as drones, sweeping robots, and automated vehicles.

In 2012, Ramesh Raskar *et al.* at Massachusetts Institute of Technology used a streak camera and an ultrafast laser to detect the target position and recover the shape of a hidden object with a back-projection algorithm [2]. They first proposed NLOS detection based on time of flight (TOF). Ellipsoid mode decomposition and fast back-projection algorithm have been presented to optimize the back-projection algorithm [3], [4]. For selecting features, Laplacian of Gaussian (LoG) and Difference of Gaussian (DoG) have been applied on the voxel space to enhance the contrast [5]. A single-photon avalanche diode (SPAD), an intensified charged coupled device (ICCD), and a two-dimensional digital camera have been used to measure scattered light [6]–[9]. A light-cone transform algorithm, Fermat flow, and phase-field virtual wave optics have been proposed to reconstruct the details of hidden objects [10]–[12].

For some applications, position information of objects is more useful than their features [13]. Daniele Faccio *et al.* used a SPAD array to record photons and located a hidden object based on photon timing information in 2016 [13], [14]. Their efficient measurement method makes it possible to track a moving object. In 2017, they used a scanning SPAD detector and a pulsed laser to detect a hidden person at a range of more than 50 m [15]. In this method, TOF of photons recorded by SPAD is used to recognize the likely positions of an object, which form an ellipse. The position of the object can be determined by locating the intersection of two or more ellipses with different focal points. The TOF has been extracted by Gauss fitting in previous work, which might be problematic without manual identification of scattering sources of interest in the presence of noise.

In this study, we propose a Gauss filtering algorithm to extract the TOF of photons accurately, robustly, and automatically. In order to simulate the NLOS location of a hidden object, we construct a model of photon flight by deriving the scattered signal. Using a scattering process characterized by the bidirectional reflectance distribution function (BRDF), the target object is discretized to derive the power of photons scattered back to the detector via this hidden object, thus making the simulated waveform more realizable and accurate than the isotropic spherical propagation model [2]. Then we perform simulations using the model. The hidden object can be tracked by simulated data with the Gauss filtering algorithm based on ellipse location. Compared with the fitting approach, this proposed positioning algorithm is capable of filtering out invalid data and noise, preserving more waveform information to improve location accuracy and stability without a prior information. Compared with the contrast enhancement algorithm (LoG and DoG) [5], the proposed Gauss filtering algorithm is applied to the time dimension rather than voxel space. Also, an experiment is implemented and demonstrates that the proposed filtering method is more robust against residual background disturbance. The proposed approach does not rely on manual identification of the signal of interest to avoid the interference of noise and residual background, and thus could be suitable for wide application in automatic NLOS detection.

This paper is structured as follows: the scattered signal is derived, and the locating strategy and the model of photon flight are illustrated in Section 2. In Section 3, we compare the Gauss filtering method with the Gauss fitting algorithm with respect to location errors under the influence of noise. In Section 4, we investigate how positioning accuracy varies with the parameters of equipment and algorithm. The advantages of the filtering algorithm are proved experimentally in Section 5. We summarize the simulation and experimental results in Section 6.

2. Model of NLOS Location

An accessible target can be imaged directly. However, a hidden target that cannot be imaged directly can be depicted by active probing. As shown in Fig. 1, an object is shielded by an obstacle on its left-hand side, and a wall acts as a mirror conveying information from the hidden area to the visible area [6]. The informative photons can be measured by a sensitive instrument such as the SPAD array [13].

In this section, we discuss the propagation process of photons from laser to detector, and analyze the variation of irradiance intensity with direction. This improved model forecasts the returning

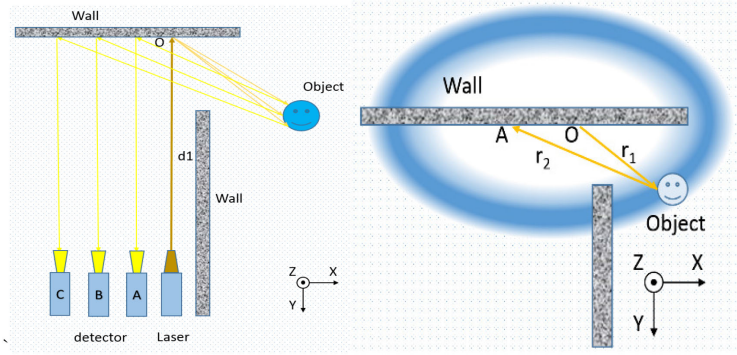

(a) (b)

Fig. 1. (a) Model of NLOS detection viewed from above. (b) Principle of positioning. All the possible positions located by a given TOF form an ellipse whose focal points are point *A* and point *O*. To determine the site by intersecting at a point, two or more ellipses are needed.

signal, and can also be used as a reference for selecting the instrument which is used to detect the scattering photons.

2.1 Method of Ellipse Location

The process is divided into four procedures. (1) Pulses from a collimated laser hit the wall at point *O* directly. (2) Scattered light from point *O* of the wall is transmitted to the hidden object as a spherical wave with intensity that follows a radial Gauss distribution, whose peak value varies with emergence angle according to the BRDF. (3) Light propagated to the target scatters back again toward the wall. (4) The intensity at point *A* is measured by a detector via transfer of the third-order scattered light back to the SPAD [16]. The distance traveled by the light in the first and last procedures can be measured in advance because point *O* and point *A* are visible. The time taken by the second and third procedures provides information about the position of the target, and can be obtained by subtracting the time taken by the first and last procedures from the whole time. Thus, TOF corresponding to r_1 and r_2 can be extracted from the returned signal. The probable positions of the hidden object form an ellipse that fits the distance of r_1 and r_2, as shown in Fig. 1(b). The object can be located by transforming the TOF to the distances r_1 and r_2. As shown in Fig. 1(a), there should be three ellipses defined by signals recorded by the three detectors. Because the position of the hidden object is included on each of these three ellipses, we can locate the hidden object by determining the intersection of the three ellipses. If the probability of a given position of the hidden object is related to the number of photons, the most probable position is regarded as the location of hidden object.

These optical procedures can be classified into two categories. The propagation between two surfaces is the irradiation model, and the scattering phenomenon on rough surfaces is the general scattering model. The irradiation model applies four times in the whole process, and, correspondingly, the scattering model applies three times between these four irradiating procedures. Apparently, in the real world, not all photons travel according to the path given above and are received by detectors; nevertheless, this is not weighted in our method. The power received by a detector after fourth- or higher-order scattering is much less than third-order-power, so it is ignored in our simulation. The signal produced by a visible object has almost no impact on positioning, because this interference signal does not fit the geometrical condition. Specifically, it has no reflection in the area of joint probability distribution, as hidden object is sought only in the area that is out of sight. As an advantage over the fitting algorithm, there is no disturbance to the target signal caused by unstable background or visible objects when filtering processing is used.

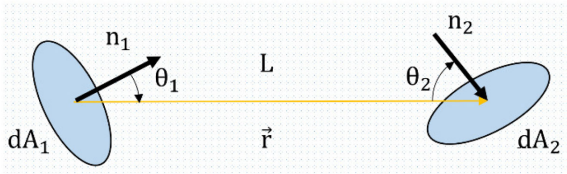

Fig. 2. Irradiation model.

2.2 Irradiation Model

As illustrated in Fig. 2, a beam from surface dA_1 irradiates surface dA_2 with radiosity L. The irradiance E on surface dA_2 can be calculated by definition.

$$E = \frac{df}{dA} \tag{1}$$

where

$$\mathrm{d}\phi = L d\Omega dA^{\perp} \tag{2}$$

$$d\Omega = \frac{\cos\theta_2 dA_2}{\left\|\vec{r}\right\|^2} \tag{3}$$

$$dA^{\perp} = \cos\theta_1 dA_1 \tag{4}$$

$$\cos\theta_1 = \left|\cos\left\langle\vec{n_1}, \vec{r}\right\rangle\right| \tag{5}$$

$$\cos\theta_2 = \left|\cos\left\langle\vec{n_2}, \vec{r}\right\rangle\right| \tag{6}$$

Therefore,

$$\mathrm{E} = \frac{\mathrm{L}d\Omega dA^{\perp}}{\mathrm{dA_2}} = \frac{\mathrm{L}\cos\theta_2\cos\theta_1 dA_1}{\left\|\vec{r}\right\|^2} \tag{7}$$

where $\vec{r}$ is a vector from dA_1 to dA_2, θ_1 (θ_2) is the angle between $\vec{r}$ and the normal of dA_1 (dA_2), Φ is the luminous flux, and Ω is the solid angle. This model shows a means to calculate the irradiance and reveals the way power attenuates with propagation in a direction.

2.3 General Scattering Model

As shown in Fig. 3, the differential radiosity dL varies with scattering direction $\vec{v}$ when an anisotropic plane is irradiated by a beam from direction $\vec{l}$ with differential irradiance dE. The ratio of dL and dE is the BRDF.

$$f\left(\vec{l}, \vec{v}\right) = \frac{dL\left(\vec{v}\right)}{dE\left(\vec{l}\right)} \tag{8}$$

The BRDF depends on the optical properties of the material surface. The distribution of scattered light can be deduced from a given BRDF and the incident light. The BRDF of an ideal Lambert reflector is a constant. Many materials have near-Lambertian opaque surfaces, and f does not vary much with $\vec{l}$ or $\vec{v}$, especially for the wall and clothes. The BRDF of the wall and clothes measured experimentally is 0.2579 and 0.1284, and recorded as f_{w} and f_{c}, respectively. The relative distribution of BRDF affects the trend of returned signals, while the magnitude of BRDF is not

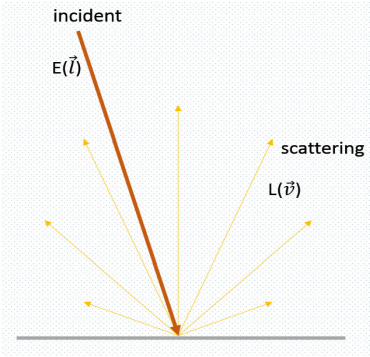

Fig. 3. Model of scattering.

necessary information in the locating process. The simulation result with experimental BRDF can be used as a reference to help select the instrument.

2.4 Scattering Model of Object Surface

The power of a Gaussian pulse is written as

$$P_0(t) \sim AN(\mu, \sigma) \tag{9}$$

The irradiance E_1 and radiosity L_1 of point O on the wall is given by

$$E_1\left(t + \frac{d}{c}\right) = \frac{P_0(t)}{S_O} \rightarrow E_1(t) = \frac{P_0\left(t - \frac{d}{c}\right)}{S_O} \tag{10}$$

According to the scattering model described in Section 2.2,

$$L_1 = f_w E_1 \tag{11}$$

The laser and detectors are 20 m from the wall, and the distance is represented by d. S_O is the area of the spot irradiated by the laser on the wall. S_A is the area measured by detector A. A, μ, and σ are parameters of the Gaussian pulse determined by laser.

As shown in Section 2.1, the irradiance on a surface element S_{1_i} irradiated by point O is given by

$$E_{2i}\left(t + \frac{r_{1i}}{c}\right) = \frac{L_1 \cos\theta_{a1i} \cos\theta_{b1i} S_O}{\left\|\vec{r}_{1i}\right\|^2} \tag{12}$$

$$L_{2i}(t) = f_c E_{2i}(t) = \frac{f_c f_w P_0\left(t - \frac{d+r_{1i}}{c}\right) \cos\theta_{a1i} \cos\theta_{b1i}}{\left\|\vec{r}_{1i}\right\|^2} \tag{13}$$

where

$$\cos\theta_{a1i} = \left|\cos\left\langle \vec{n_{wall}}, \vec{r_{1i}} \right\rangle\right| \tag{14}$$

$$\cos\theta_{b1i} = \left|\cos\left\langle \vec{n_{s1i}}, \vec{r_{1i}} \right\rangle\right| \tag{15}$$

The irradiance on point A irradiated by S_{1_i} is given by

$$E_{3i}\left(t + \frac{r_{2i}}{c}\right) = \frac{L_{2i} \cos\theta_{a2i} \cos\theta_{b2i} S_{1i}}{\left\|\vec{r}_{2i}\right\|^2} \tag{16}$$

$$\cos\theta_{a2i} = \left|\cos\left\langle \vec{n_{s1i}}, \vec{r_{2i}} \right\rangle\right| \tag{17}$$

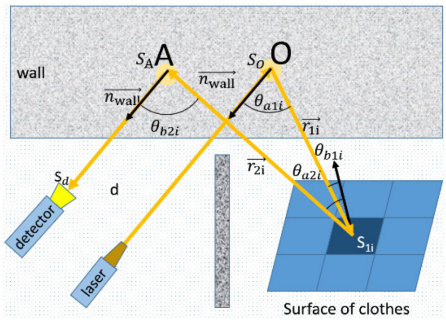

Fig. 4. Schematic diagram of parameters. The surface of the hidden object is separated into a large number of tiny segments. The parameters of each segment are regarded as constants.

$$\cos\theta_{b2i} = \left|\cos\left\langle \vec{n_{wall}}, \vec{r_{2i}}\right\rangle\right| \tag{18}$$

The extended object is regarded as a combination of tiny segments instead of a single-point target [13]. Photons scattered at different parts of the hidden object travel through different paths back to the detector, therefore,

$$E_3 = \iint_{s_1} \frac{f_c f_w P_0 \left(t - \frac{d+r_{1i}+r_{2i}}{c}\right) \cos\theta_{a1} \cos\theta_{b1} \cos\theta_{a2} \cos\theta_{b2}}{\left\|\vec{r}_{1i}\right\|^2 \left\|\vec{r}_{2i}\right\|^2} ds \tag{19}$$

Irradiance of the detector, which is perpendicular to the wall, can be obtained by the same method:

$$E_4\left(t + \frac{d}{c}\right) = \frac{L_3 \cos\frac{\pi}{2} \cos\frac{\pi}{2} S_A}{d^2} = \frac{f_w E_3 S_A}{d^2} \tag{20}$$

Finally, the power received by the detector can be obtained:

$$P(t) = E_4(t) S_d \tag{21}$$

3. Simulation Result and Location

3.1 Setting of Simulation Parameters

Based on the model described in Section 2, we perform simulations to validate the effectiveness of the proposed filtering method. In the simulations, the power of the laser is 750 mW, frequency is 80 MHz, wavelength is 1530 nm, and the full width at half maximum (FWHM) of a pulse is 70 ps. The energy of a Gaussian pulse is

$$A = (750\ \text{mw}) / (80\ \text{MHz}) = 9.375 \times 10^{-9} J \tag{22}$$

The power is half of the peak when $t_{0.5} = \mu \pm \sqrt{2 \ln 2 \sigma^2}$. Therefore,

$$FWHM = 2\sqrt{2 \ln 2 \sigma^2} \rightarrow \sigma = \frac{70\ \text{ps}}{2\sqrt{2 \ln 2}} = 29.73\ \text{ps} \tag{23}$$

According to the Pauta criterion, almost the entire energy of a pulse is concentrated in the 3σ interval $[\mu - 3\sigma, \mu + 3\sigma]$. The pulse occurs at zero time, and thus $\mu = 3\sigma$. The diameters of the laser beam and the detected area on the wall are 0.07 m and 0.1 m, respectively. These parameters are set referring to an experimental laser source. It is verified in Section 4 that the width of the laser pulse is not necessary a priori information.

The hidden object is substituted with an upright plane of 0.3 m $\times$ 1.6 m placed at coordinates (4, 2, 0), and perpendicular to the x-axis. Three points A(–0.5, 0, 0), B(–1, 0, 0), and C(–1.5, 0, 0)

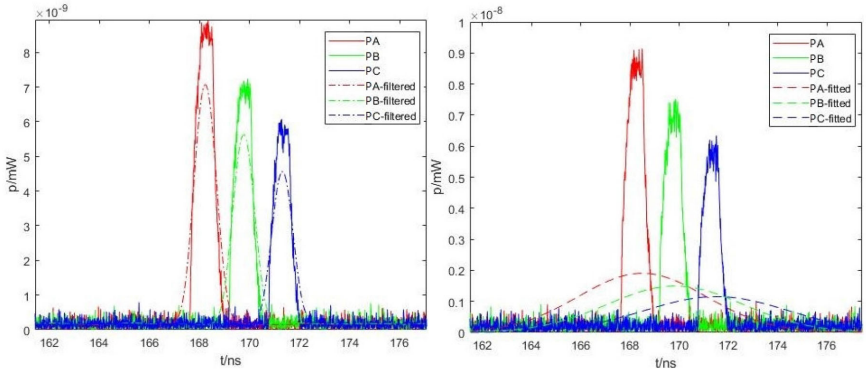

Fig. 5. The original power is illustrated as solid lines, which are scattered from the same target in the same position. The FWHMs of scattered pulses are 0.88 ns, 0.82 ns, and 0.79 ns, recorded by virtual detector A, detector B, and detector C, respectively. (a) The signals represented by the dashed lines are filtered by a Gauss filter with an interval of 0.8 ns. The calculation method is given in Eq. 24. (b)The curves represented by the dashed lines are Gauss fitted without selecting the fitting interval manually.

on the wall are imaged to three detectors, respectively. We note that there is only one object in our simulation, which is placed in different positions to validate our method.

3.2 Positioning With a Gauss Filter

A 10-dB noise level is added to the ideal echo to simulate the noise of environment and dark count rate of the detector. The returned power simulated by numeral calculations is shown in Fig. 5.

The returned power is an accumulation of Gaussian pulses with different attenuation degrees at different times due to different paths and directions. The waveform of the signal pulse depends on the shape of the hidden object. Effects of the object's shape on the signal waveform and locating result are analyzed in Section 4. The energy received in a given period of time may be less than a photon, but that does not mean that the data or method has failed. A train of pulses would be sent from the laser in an experiment. The returned signal is a result of repeated measurement, and it is also a statistical process. Referring to the method proposed by Daniele Faccio *et al.* [13], the power corresponding to each instant is related to the probability of a given position being the location of the hidden object. The TOF can be transformed into the sum of r_1 and r_2. A search strategy is carried out on the plane $z = 0$ in the hidden area according to the obtained sum. Based on the fact that the probability density of TOF is proportional to the power received at the given moment, the location probability density distribution p_A can be obtained from power P_A by referring to the geometrical relations in Fig. 1(b), as shown in Fig. 6(a). Fig. 6(d) shows that the joint probability density distribution calculated by multiplying three probability density distributions (p_A, p_B, and p_C) using original data. With the coordinate of maximum probability taken as the position of the target, the simulated detected location result (shown as a black cross) presents an evident error from the real one (shown as a red circle).

The high power scattered by a part of an object cannot reflect the coordinate of the geometrical center. Oscillations on the peaks of the solid curves shown in Fig. 5 would result in an instability of location by disturbing the extrema. In order to approach the coordinate of the geometrical center, the curves should be smoother and the weight of the signal should be adapted. In this case, a Gauss filter is applied to process the raw data with an interval of h. The principle is expressed by Eq. 24:

$$P'(t) = \int_{t-h}^{t+h} P(\tau) \times \frac{1}{\sqrt{2\pi}\sigma} \exp\left[-\frac{(\tau - t)^2}{2\sigma^2}\right] d\tau \tag{24}$$

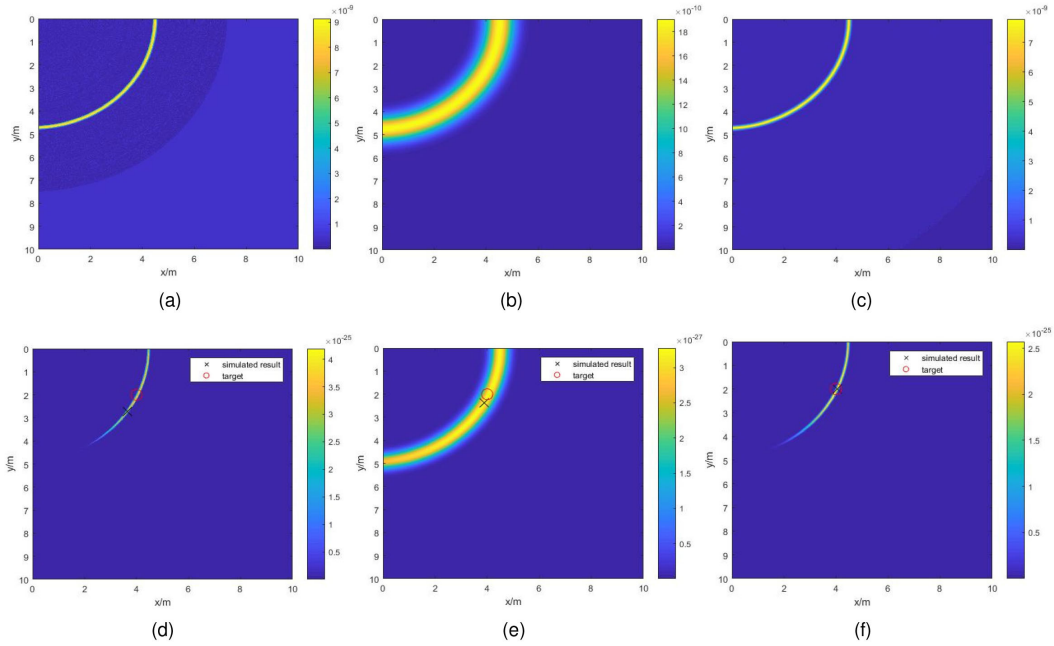

Fig. 6. Probability density distribution. Probability density distribution (p_A) according to (a) the raw signal P_A received by detector A, (b) the Gauss fitted signal, and (c) the signal Gauss filtered with $h = 0.65$ ns. The joint probability density distribution according to (d) the original signal, (e) the Gauss fitted signal, and (f) the Gauss filtered signal. The detected coordinates are (3.64, 2.73, 0), (3.88, 2.38, 0), and (4.04, 2.00, 0), shown by black crosses.

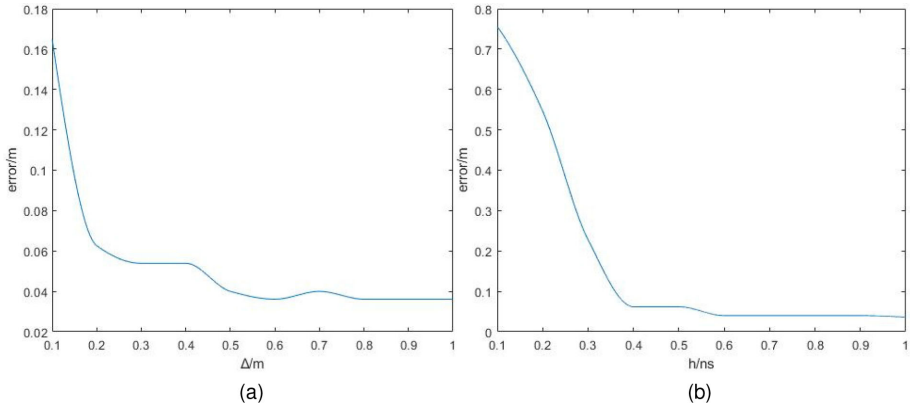

Fig. 7. (a) Positioning error as a function of Δ. (b) Positioning error as a function of h.

where P is the original signal recorded by the detector, h is the filtering interval, σ is variance, and P' is the filtered signal. According to the Pauta criterion, $h = 3\sigma$. The value of h is optimized in simulation as mentioned in Fig. 7(b). Referring to the principle proposed by Gariepy *et al.* [13], P' shows the probability distribution of TOF.

The Gauss fitting approach is also used by the team of Daniele Faccio for signal processing. For comparison, the original signal P is fitted to Gauss function with least-square method using Eq. 25:

$$P' \propto \exp\left(-\frac{\left((r_1 + r_2)/c - \langle t \rangle\right)^2}{2\sigma^2}\right) \tag{25}$$

where $(r_{1+} r_2)/c$ represents the time dimension of fitting the processed signal, and $<t>$ and σ can be calculated with the least-square method. The waveforms are modified to Gauss distribution by this fitting algorithm. Without identifying the useful signals manually, these Gauss-distributed waveforms would be distorted because of noise and unstable background.

The filtered signal and fitted signal are presented as the dashed curves in Fig. 5(a) and (b). As one can see, without selecting the fitting interval manually, the automatic fitted signal is over-dispersed under the influence of noise. On the contrary, the filtering algorithm can retain more information about the waveform, and using signals reflecting the authentic waveform helps achieve an undistorted location.

The deviation caused by data fluctuations are eliminated by these two kinds of smoothing operations. The filtered joint probability density distribution (p') is illustrated in Fig. 6(c), and the fitted one is shown as Fig. 6(b). The final results of position detection are presented in Figs. 6(d)–6(f), with the maximum value points of the probability density distributions regarded as the detected position. The location result using the filtered signal is closer to the real position than either of those using the raw or fitted signal. Thus, the Gauss filter can be applied for real-time detection without artificial judgment of signals of interest.

Additionally, although the returned power is used to locate the target, the trend of the data is much more useful than the magnitude. In other words, waveform is the only valuable information for positioning and it is influenced by the shape of object and the BRDF distribution of the surface of the object. The numerical value of the power can be reflected by the counts of photons captured by the SPAD experimentally.

4. Investigation of Positioning Performance

Positioning accuracy could be influenced by many factors, such as environmental noise and the stability and accuracy of the equipment. This section shows how positioning accuracy varies with the settings of the equipment. The configuration and parameters are the same as those mentioned in Section 3.

In general, the distance between detectors (Δ) is limited by the experimental site or application scenario. However, short distances would result in similarity of the datasets received by detectors. Each different signal contains additional information. Fig. 7(a) indicates the change in location accuracy with increasing Δ. From these results, 0.6 m is chosen as an appropriate distance.

The filtering algorithm has an advantage over the fitting algorithm in retaining the waveform information. The size of the interval (h) where the Gauss filter is applied is an important parameter that determines the positioning effect by influencing the retention and smoothness of the waveform. The size of the interval should be suitable to filter out high-frequency signals and retain enough effective information. An effective and stable value of h is 0.65 ns, as shown in Fig. 7(b), which is also used in the experiment.

In order to study the influence of pulse width on locating results, we simulated a hidden object situated at (4, 2, 0) and tested different pulse widths. The change of the locating result with FWHM of the laser source is shown in the table below. In general, the simulation result shows that the FWHM of a laser does not have an obvious influence on the locating result. Despite this, the narrow laser pulse is preferred to avoid the aliasing caused by wide pulses.

We also studied the effect of the shape of the hidden object on the locating accuracy. The size of the rectangular object was changed to 0.2 m $\times$ 1.8 m, 0.5 m $\times$ 1.5 m, and 0.8 m $\times$ 1.2 m, in order. The simulation results are shown in Fig. 8. It is obvious that the widths of scattered signals are largely influenced by the shape of the object, but the locating results changed little. It can be inferred from simulation that the objects of similar size but different shapes can be located by our method with almost same accuracy.

To study the relation between object size and location accuracy, objects of different sizes at the same position are located through the simulation. The object is simulated by a square surface, of which the side length is taken as the variable to characterize the object size.

TABLE 1
Locating Result for Various Full Width at Half Maximum (FWHM) of Laser

FWHM of laser (ps)	40	50	60	70	80	90
Locating result (m)	(4.02,2.03,0)	(4.04,1.99,0)	(4.02,2.04,0)	(4.04,2.00,0)	(4.02,2.08,0)	(4.03,2.03,0)

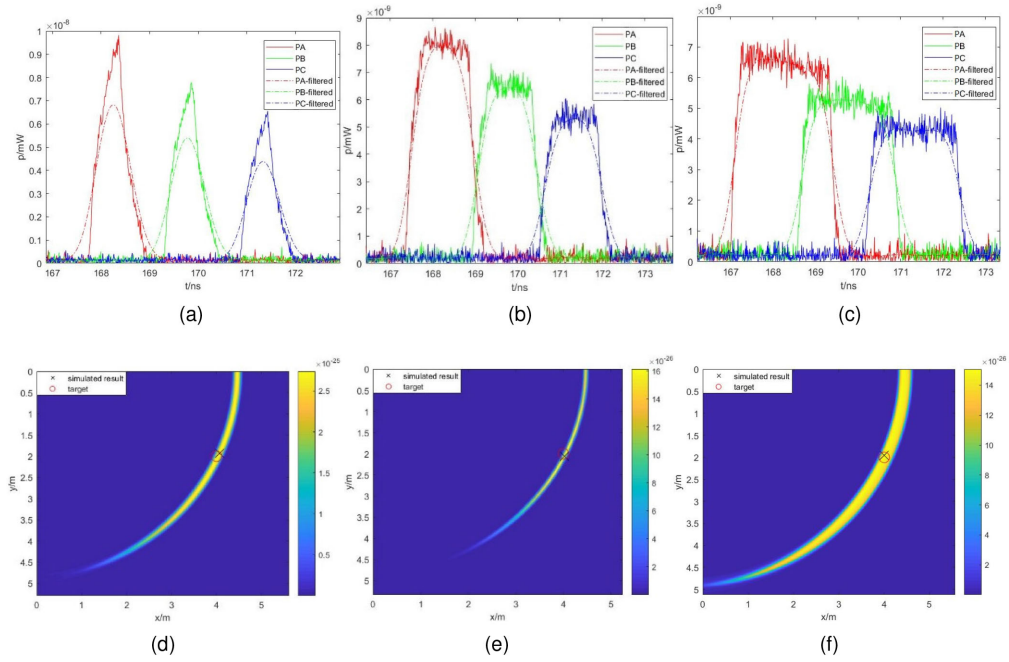

Fig. 8. The detected signals scattered by objects of (a) 0.2 m × 1.8 m, (b) 0.5 m × 1.5 m, and (c) 0.8 m × 1.2 m. The locating results are (d) (4.02, 2.06), (e) (4.07, 1.93), and (f) (4.00, 1.95) for the objects in (a), (b), and (c), respectively.

The simulation results are shown in Fig. 9, from which it can be seen that the location accuracy declines with the increase in side length. This could be attributed to the decreased signal contrast and signal-to-noise ratio with the increase in object size. In our model, the big object can be regarded a combination of several small objects. So, it can be concluded that the wider signals caused by the increasing object size enhance the difficulty of extracting TOFs.

To further check the superior positioning performance of the Gauss filter over the fitting algorithm, another simulation was performed testing multiple locations. The target was situated at each coordinate of a 5 × 5 array from (1,1,0) to (5,5,0) successively, and the distance between adjacent coordinates is 1 m. The positioning error of each coordinate is shown in Fig. 10.

Positioning errors and frequency histograms with the Gauss fitting algorithm are shown in Figs. 10(a) and 10(b), while those with Gauss filtering are presented in Figs. 10(c) and 10(d). It can be seen that the target can be located in the search area within a 0.12 m allowance range using the Gauss filtering approach. The mean and standard deviation of errors decreased from 0.3106 m and 0.3010 m with the fitted signal to 0.0684 m and 0.0245 m, respectively, with the filtered signal. That means that the positioning accuracy and reliability achieved by

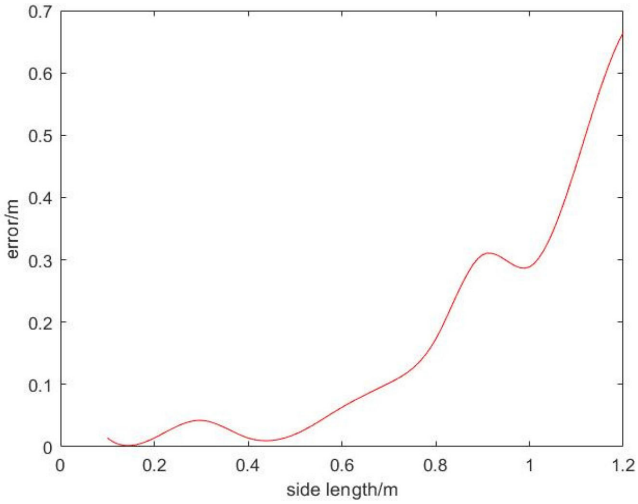

Fig. 9. Relation between location error and side length.

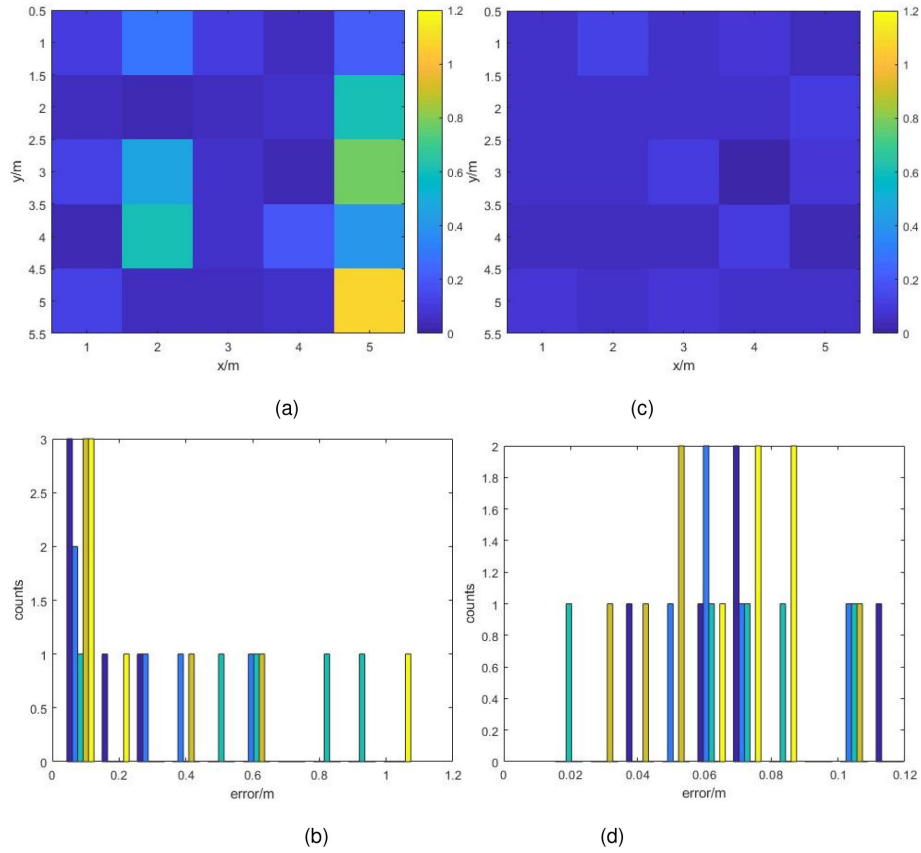

Fig. 10. (a) Positioning error and (b) frequency histogram of error at each coordinate with Gauss fitting algorithm. (c) Positioning error and (d) frequency histogram of error at each coordinate with Gauss filtering algorithm.

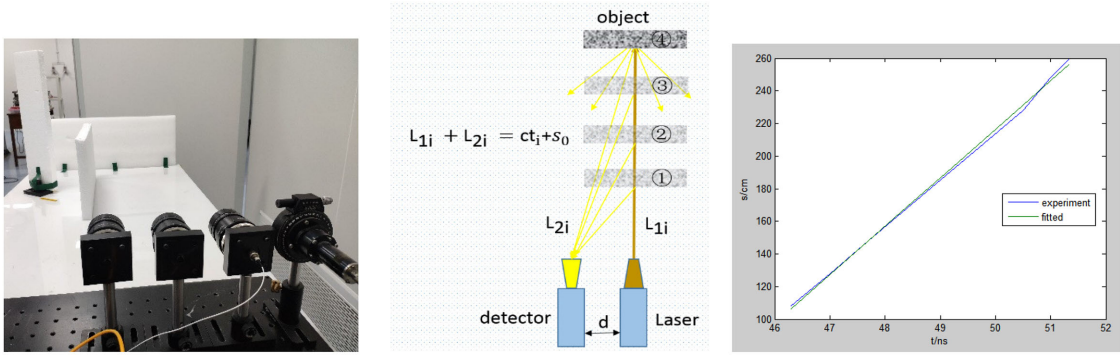

(a) (b) (c)

Fig. 11. (a) Experimental setup. (b) Matching process. (c) Fitting result.

filtering are better than those achieved by the fitting algorithm. This simulation further demonstrates that the filter approach is better than fitting with regard to positioning accuracy and reliability.

5. Experimental Results

Our method is also verified by experiment at a range of 1.3 m ($d = 1.3$ m). The detectors are separated at a distance of 0.075 m ($\Delta = 0.075$ m). The experimental equipment includes a superconducting nanowire single photon detector (SNSPD), a time to digital converter (TDC), a pulsed laser source (1531 nm wavelength, 10 W peak power, 20 MHz repetition frequency, 0.4 ns FWHM), and three lenses (50 mm focal length). As shown in the left of Fig. 11(a), the object is a cuboid foam that is 40 cm high, 10 cm wide, and 2 cm thick. The time resolution of the TDC is set to 50 ps in this experiment.

Considering that the optical path in fiber and equipment cannot be measured directly, we measured the length ($L_{1_i} + L_{2_i}$) that photons fly in free space as shown in Fig. 11(b). The object was set toward the laser at different distances (L_{1_i}). The optical paths ($L_{1_i} + L_{2_i}$) in free space are matched with the times of signal peak by linear fitting, as presented in Fig. 11(c) using Eq. 26, as follows

$$\mathrm{s(cm)} = 29.7\,\mathrm{(cm/ns)} \times \mathrm{t(ns)} - 1269.1\,\mathrm{(cm)} \tag{26}$$

There is an error of 0.67% between the measured speed of light and the normal value, which might be caused by the instability of the equipment and errors of measurement. The root mean square error (RMSE) and coefficient of determination (R^2) are 2.07 cm and 0.9983, respectively, demonstrating that the fitting result is reliable.

The photons scattered by the hidden object are extracted from the background by subtracting the background signal from the detected signal. Fig. 12 shows an example of the signal recorded by three detectors, when the NLOS object is hidden at the coordinate (0.47, 0.31). In order to obtain the TOF, the data is processed with both the Gauss fitting algorithm and Gauss filter, and the results are compared.

The signals of interest appear around the time of 5 ns, which provides information about the position of target. According to the geometrical condition of the optical path, the data in the red box (shown as the second and third rows of Fig. 12) correspond to the TOF of photons scattered by the NLOS object, and the data outside red box have no contribution to the search process. The narrow peaks on the left side of the red box are probably caused by the instability of the background in the extraction procedure, which is the main interference in the Gauss fitting algorithm. Our method is able to preserve the waveform information in the red box in the presence

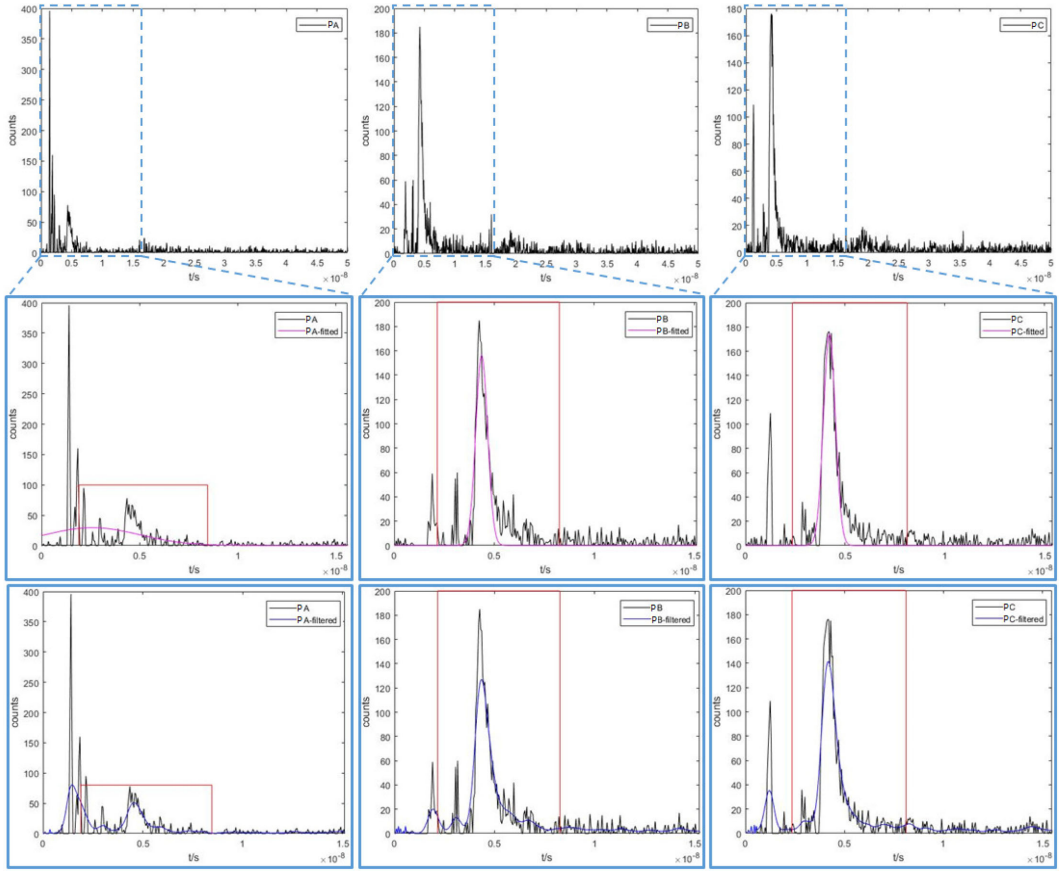

Fig. 12. The three columns show the signals recorded by three detectors, respectively. The FWHMs of scattered pulses are 0.65 ns, 0.58 ns, and 0.91 ns, recorded by detector A, detector B, and detector C, respectively. The three rows present the original signal of the target extracted from the background, the Gauss fitted signal, and the Gauss filtered signal with interval of 0.65 ns ($h = 0.65$ ns), left to right.

of an unstable background, and eliminate the influence of noise without the artificial identification of a target area (the red box). Specifically, if a Gauss fitting algorithm is performed on the whole data without manual judgment, the signal interval (red box) would be influenced by noise and background (especially the signal measured by detector A). Thus, the number of Gauss terms should be set as prior information determined by judgment. However, the Gauss filtering algorithm suppresses noise jamming and preserves the informative waveforms without the requirement of advance identification of an informative interval. As a priori information, the number of Gauss terms is not required for the filtering algorithm. Referring to our simulation, the Gauss filtering approach is performed on the data with an interval of 0.65 ns ($h = 0.65$ ns).

Based on the processed signals, we can locate the hidden object. As previous studies have shown [13], the photon counts recorded by detectors in each instant are related to the probability of a given TOF. The probability of a signal TOF can be transformed to the probability of an optical path by referring to Eq. 26. The location probability density distribution is obtained from the optical path probability according to the ellipse location strategy (see Fig. 1). We search for the target in a region with a height of 0.2 m. The joint probability distribution is obtained by multiplying three probability density distributions, according to signals recorded by three detectors. The coordinate of maximum probability is taken as the position of target, represented by the black crosses for the filtered signal and yellow diamonds for the fitted signal, respectively, while the real positions of the objects are displayed as red circles. These results show that not only the accuracy (Fig. 13(a))

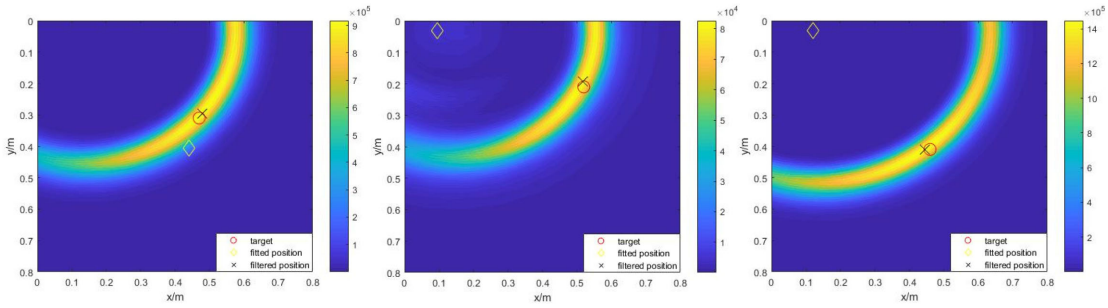

Fig. 13. The target is placed at the coordinates (0.47, 0.31), (0.52, 0.21), and (0.46, 0.41), shown as red circles. The location results using the fitting algorithm and using the filtering algorithm are (0.44, 0.40), (0.095, 0.03), and (0.12, 0.03) and (0.48, 0.29), (0.52, 0.19), and (0.44, 0.41), which are shown as yellow diamonds and black crosses, respectively.

but also the stability (Figs. 13(b) and 13(c)) of the location results using filtered signals is better than that of the results using fitted signals.

As the experimental results show, the location of the hidden object by the Gauss fitting algorithm is distorted in the presence of noise and unstable background. It has a poor anti-interference ability without manual intervention. However, the NLOS object can be located automatically using the Gauss filtering algorithm, and the error is within 0.02 m. The filtering algorithm performs better than the fitting algorithm in an experimental environment with noise and unstable background. Even without artificial identification of the signal interval, it is possible to locate the NLOS object automatically and rapidly by using our proposed Gauss filtering method.

6. Conclusion

In this paper, a photon flight model of scattering and propagation processes is used to calculate the power of signals scattered by a hidden object and received by detectors. The returned signal can be simulated given the BRDF and surface information of the hidden object. By processing the signals with a Gauss filter, a human-sized object is located accurately in a large range (i.e., an object can be located in a 5 m $\times$ 5 m area within a tolerance of 12 cm). Moreover, the influence of the environment and equipment configuration on positioning has been analyzed to determine the appropriate parameters. Some deviation is unavoidable because a point is located by using the data produced by a surface. Therefore, this method is effective only when the distance between the positioning coordinate and the geometric center of the object is within the size of the hidden object. Finally, the stability of our method is verified by experiment at a range of 1.3 m. Compared with the fitting algorithm, the filtering algorithm has greater potential for applications in real-time location determination due to its lower complexity.

References

[1] A. Beckus, A. Tamasan, and G. K. Atia, "Multi-modal non-line-of-sight passive imaging," *IEEE Trans. Image Process.*, vol. 28, no. 7, pp. 3372–3382, Jul. 2019.

[2] A. Velten, T. Willwacher, O. Gupta, A. Veeraraghavan, M. G. Bawendi, and R. Raskar, "Recovering three-dimensional shape around a corner using ultrafast time-of-flight imaging," *Nature Commun.*, vol. 3, no. 3, p. 745, 2012. [Online]. Available: https://www.nature.com/articles/ncomms1747

[3] C. F. Jin, J. H. Xie, S. Q. Zhang, Z. J. Zhang, and Y. Zhao, "Reconstruction of multiple non-line-of-sight objects using back projection based on ellipsoid mode decomposition," *Opt. Express*, vol. 26, no. 16, pp. 20089–20101, 2018.

[4] V. Arellano, D. Gutierrez, and A. Jarabo, "Fast back-projection for non-line of sight reconstruction," *Opt. Express*, vol. 25, no. 10, pp. 11574–11583, 2017.

[5] L. Martin and A. Velten, "Feature selection and back-projection algorithms for nonline-of-sight laser–gated viewing," *J. Electron. Imag.*, vol. 23, no. 6, 2014, Art. no. 063003.

[6] K. D. Xu *et al.*, "Image contrast model of non-line-of-sight imaging based on laser range-gated imaging," *Opt. Eng.*, vol. 53, no. 6, 2014, Art. no. 061610.
[7] M. Laurenzis and A. Velten, "Nonline-of-sight laser gated viewing of scattered photons," *Opt. Eng.*, vol. 53, no. 2, 2014, Art. no. 023102.
[8] M. Buttafava *et al.*, "Non-line-of-sight imaging using a time-gated single photon avalanche diode," *Opt. Express*, vol. 23, no. 16, pp. 20997–21011, 2015
[9] J. Klein, C. peters, J. Martin, M. Laurenzis, and M. B. Hullin, "Tracking objects outside the line of sight using 2D intensity images," *Scientific Rep.*, vol. 6, 2016, Art. no. 32491.
[10] M. O'Toole, D. B. Lindell, and G. Wetzstein, "Confocal non-line-of-sight imaging based on the light-cone transform," *Nature*, vol. 555, no. 7696, pp. 338–341, 2018.
[11] S. Xin, S. Nousias, K. N. Kutulakos, A. C. Sankaranarayanan, S. G. Narasimhan, and I. Gkioulekas, "A theory of fermat paths for non-line-of-sight shape reconstruction," in *Proc. IEEE Conf. Comput. Vision Pattern Recognit.*, 2019, pp. 6800–6809.
[12] X. Liu *et al.*, "Non-line-of-sight imaging using phasor-field virtual wave optics," *Nature*, vol. 572, pp. 620–623, 2019.
[13] G. Gariepy, F. Tonolini, R. Henderson, J. Leach, and D. Faccio, "Detection and tracking of moving objects hidden from view," *Nature Photon.*, vol. 10, no. 1, pp. 23–26, 2016.
[14] G. Gariepy *et al.*, "Single-photon sensitive light-in-fight imaging," *Nature Commun.*, vol. 6, 2015, Art. no. 6021.
[15] S. Chan, R. E. Warburton, G. Gariepy, J. Leach, and D. Faccio, "Non-line-of-sight tracking of people at long range," *Opt. Express*, vol. 25, no. 9, pp. 10109–10117, 2017.
[16] M. laurenzis, F. Christnacher, and A. Velten, "Study of single photon counting for non-line-of sight vision," *Proc. Adv. Photon Counting Techn. IX 94920K /Adv. Photon Counting Techn. IX.SPIE*, vol. 9492, 2015, Art. no. 94920K.